Journal of Solid State Chemistry 184 (2011) 531–535

Contents lists available at ScienceDirect

Journal of Solid State Chemistry

journal homepage: www.elsevier.com/locate/jssc

Magnetic properties of barium uranate $Ba_2U_2O_7$

Akio Nakamura [a], Yoshihiro Doi [b], Yukio Hinatsu [b,*]

[a] Advanced Science Research Center, Japan Atomic Energy Agency (JAEA), Tokai-mura, Ibaraki 319-1195, Japan
[b] Division of Chemistry, Graduate School of Science, Hokkaido University, Sapporo 060-0810, Japan

ARTICLE INFO

Article history:
Received 2 September 2010
Received in revised form
27 December 2010
Accepted 29 December 2010
Available online 5 January 2011

Keywords:
Uranium
Magnetic properties
Specific heat
Magnetic susceptibility
Optical absorption spectrum
Crystal field
Weberite-type structure

ABSTRACT

Unique magnetic properties of a ternary uranate $Ba_2U_2O_7$ are reported. Magnetic susceptibility measurements reveal that this compound undergoes a magnetic transition at 19 K. Below this temperature, magnetic hysteresis was observed. The results of the low-temperature specific heat measurements below 30 K support the existence of the second-order magnetic transition at 19 K. $Ba_2U_2O_7$ undergoes a canted antiferromagnetic ordering at this temperature. The magnetic anomaly which sets in at 58 K may be due to the onset of one-dimensional magnetic correlations associated with the linear chains formed by U ions. The analysis of the experimental magnetic susceptibility data in the paramagnetic temperature region gives the effective magnetic moment $\mu_{eff}=0.73\ \mu_B$, the Weiss constant $\theta=-10$ K, and the temperature-independent paramagnetic susceptibility $\chi_{TIP}=0.14\times10^{-3}$ emu/mole.

The magnetic susceptibility results and the optical absorption spectrum were analyzed on the basis of an octahedral crystal field model. The energy levels of $Ba_2U_2O_7$ and the crystal field parameters were determined.

1. Introduction

During fission of uranium, a variety of fission products are formed, some of which are accommodated in UO_2 fuel [1]. Among them, barium has a quite low solubility into UO_2 [2] because of its large ionic radius [3], and forms various kinds of ternary oxides [1]. So, it is very attractive to study the Ba–U–O system, and some ternary oxides such as BaU_2O_7, $BaUO_4$, and Ba_3UO_6 are known to form.

We have been interested in a compound $Ba_2U_2O_7$. This phase is formed between $BaUO_3$ and $BaUO_4$, and the valence state of uranium is pentavalent. The crystal structure of $Ba_2U_2O_7$ has been determined by X-ray diffraction and neutron diffraction methods [4].

The magnetic and optical properties of actinides are characterized by the behavior of 5*f* electrons. For the 5*f* compounds, the crystal field, spin–orbit coupling, and electron–electron repulsion interactions are of comparable magnitude, which makes the analysis of the experimental results complicated. In the case of U^{5+} compound, the situation is considerably simplified because there is no electronic repulsion interaction (the electronic configuration of U^{5+} ion is $[Rn]5f^1$). Therefore, the theoretical treatment of the U^{5+} ion is easier and we may obtain a deeper understanding of the behavior of 5*f* electrons in solids.

Previously, we briefly reported the temperature-dependence of magnetic susceptibility for $Ba_2U_2O_7$ [5]. In this study, we freshly prepared $Ba_2U_2O_7$ and measured its magnetic susceptibility in the temperature range 1.8–400 K, and specific heat in the temperature range 1.8–30 K. Because the optical absorption spectra are available [6], we will determine the energy state of the U^{5+} ion in the compound and evaluate the magnetic susceptibilities measured here.

2. Experimental

2.1. Sample preparation

The present $Ba_2U_2O_7$ was prepared by mildly reducing $BaUO_4$ in a flowing 4% H_2 in He gas atmosphere for 12–24 h at 1100–1400 °C. The starting $BaUO_4$ had been prepared by heating mixtures of $Ba(NO_3)_2$ and UO_3 powders at 800–1100 °C in oxygen atmosphere.

2.2. Analysis

2.2.1. X-ray diffraction analysis

Powder X-ray diffraction profiles were measured using a Rigaku Multi-Flex diffractometer with Cu*K*α radiation equipped

* Corresponding author.
E-mail address: hinatsu@sci.hokudai.ac.jp (Y. Hinatsu).

0022-4596/$ - see front matter © 2011 Elsevier Inc. All rights reserved.
doi:10.1016/j.jssc.2010.12.023

with a curved graphite monochromator. The data were collected by step- scanning in the angle range of $10^\circ \le 2\theta \le 120^\circ$ at a 2θ step-size of 0.02°. The X-ray diffraction data were analyzed by the Rietveld technique, using the programs RIETAN2000 [7], and the crystal structures were drawn by VESTA program [8].

2.2.2. Determination of oxygen amount

The oxygen non-stoichiometry in the sample was checked by the back-titration method [9,10]. A weighed sample was dissolved in excess cerium (IV) sulfate solution which had been standardized in advance with stoichiometric UO_2. Then the excess cerium (IV) was titrated against a standard iron (II) ammonium sulfate solution with ferroin indicator. The oxygen amount was determined for a predetermined Ba/U ratio.

2.3. Magnetic susceptibility measurements

The temperature-dependence of the magnetic susceptibility was measured at various magnetic field between 0.01 and 5.5 T over the temperature range of $1.8\ \mathrm{K} \le T \le 400\ \mathrm{K}$, using a SQUID magnetometer (Quantum Design, MPMS5S). The susceptibility measurements were performed under both zero-field-cooled (ZFC) and field-cooled (FC) conditions. The former was measured upon heating the sample to 400 K under the applied magnetic field of 0.01–5.5 T after zero-field cooling to 1.8 K. The latter was measured upon cooling the sample from 400 to 1.8 K at 0.01–5.5 T. Magnetization measurements (M–H curve measurements) were performed at 2.0 K in the applied magnetic field of $-5.5\ \mathrm{T} \le H \le 5.5\ \mathrm{T}$.

2.4. Specific heat measurements

Specific heat measurements were performed using a relaxation technique by a commercial heat capacity measuring system (Quantum Design, PPMS) in the temperature range 1.8–30 K. The sintered sample in the form of a pellet was mounted on a thin alumina plate with Apiezon for better thermal contact.

3. Results and discussion

3.1. Preparation and crystal structure

The chemical analysis of the oxygen concentration gives the formula $Ba_2U_2O_{6.993}$. In view of the error limits for this analysis, this result indicates that the specimen is oxygen-stoichiometric. The X-ray diffraction analysis shows that the $Ba_2U_2O_7$ prepared in this study crystallizes in the weberite-type Na_2MgAlF_7. It is orthorhombic with lattice parameters $a=8.162$, $b=11.301$, and $c=8.189$ Å, and the space group is *Imma*. Fig. 1 shows the crystal structure of $Ba_2U_2O_7$. Both Ba and U atoms have two different crystallographic sites. Ba1 and Ba2 have hexagonal bipyramidal and square prismatic coordinations, respectively; both U1 and U2 have the octahedral coordination. The $U1O_6$ octahedra are joined together in infinite one-dimensional $U1O_6$ chains by sharing their apical oxygens. The $U1O_6$ octahedra are tilted with respect to each other with U1–O–U1 angle of 141.4° and form a zig-zag chain running parallel to the a-axis. Each $U1O_6$ octahedron is connected with four $U2O_6$ octahedra by corner-oxygen sharing.

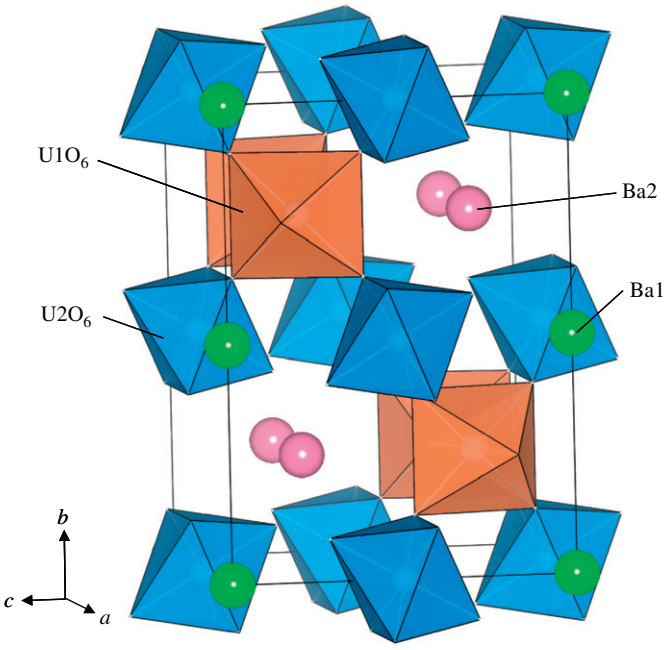

Fig. 1. Crystal structures of $Ba_2U_2O_7$.

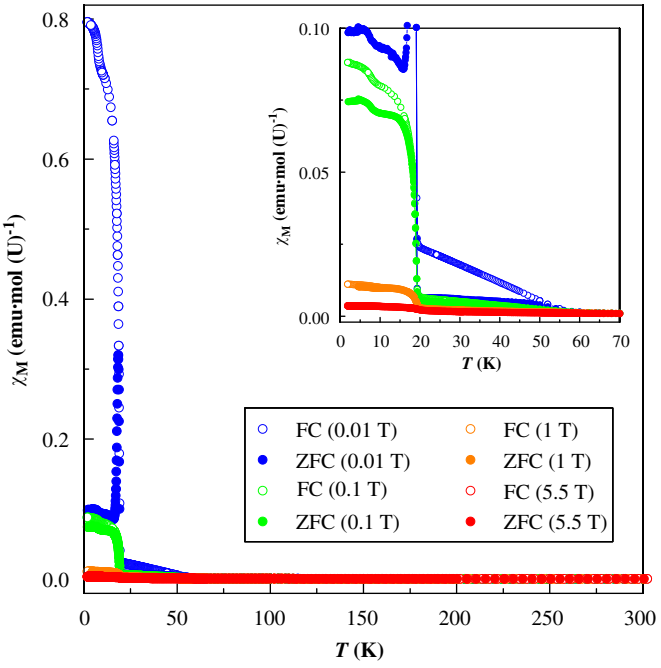

Fig. 2. Temperature dependence of magnetic susceptibility for $Ba_2U_2O_7$ at various applied magnetic field ($H=0.01$–5.5 T) in the temperature region between 1.8 and 300 K. The susceptibility is expressed per mole of U. The inset shows the detailed temperature dependence of the susceptibility below 70 K.

3.2. Magnetic properties

3.2.1. Magnetic behavior in the paramagnetic temperature region

Fig. 2 shows the temperature dependence of the magnetic susceptibility for $Ba_2U_2O_7$ measured at various magnetic field between 0.01 and 5.5 T. Above 58 K, the susceptibility does not depend on the magnetic field, and $Ba_2U_2O_7$ shows paramagnetic behavior.

Fig. 3 depicts the temperature dependence of the reciprocal magnetic susceptibility for $Ba_2U_2O_7$ in the temperature range between 1.8 and 300 K. Above 58 K, it follows a single curve. The least square fitting gives the characteristic magnetic parameters for the U^{5+} ions in the distorted octahedral sites, i.e., the effective magnetic moment $\mu_{\mathrm{eff}}=0.73\ \mu_B$, the Weiss constant $\theta=-10$ K,

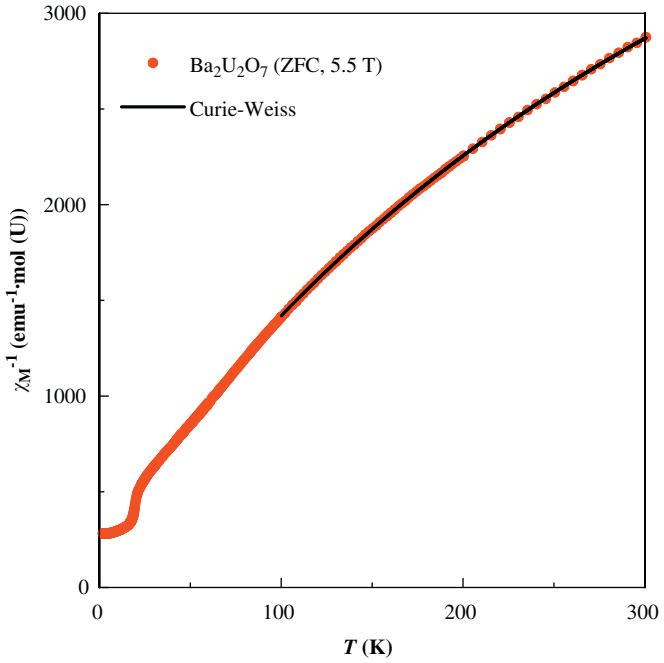

Fig. 3. The reciprocal susceptibility vs. temperature curve for $Ba_2U_2O_7$. A solid line is the Curie–Weiss fitting.

and the temperature-independent paramagnetic susceptibility $\chi_{TIP}=0.14\times10^{-3}$ emu/mole.

The effective magnetic moment of $Ba_2U_2O_7$ is much smaller than that for the moment of a free f^1 ion, U^{5+} (2.54 μ_B), which indicates that the crystal field effect on the magnetic properties of an f electron is large. Similar small magnetic moments have been reported for some U^{5+} bearing ternary oxides with the same $5f^1$ electronic configuration [11].

Since the absorption spectra are available for this compound [6], we can determine the crystal field energy levels and then calculate the magnetic susceptibility.

Fig. 4 shows the effects of perturbing the f^1 orbital energy levels successively by an octahedral field and spin–orbit coupling. In an octahedral crystal field, the sevenfold degenerate energy state of the f orbitals is split into Γ_2, Γ_5, and Γ_4 states, where Δ and Θ represent the parameters of the crystal field strengths. If spin–orbit coupling is taken into account, the Γ_2 orbital state is transformed into Γ_7, whereas the Γ_5 and Γ_4 states are split into Γ_7^* and Γ_8, and Γ_6 and Γ_8^*, respectively. The ground-state Kramers doublet is the Γ_7 state and is coupled to the excited Γ_7^* state arising from the Γ_5 orbital, by the spin–orbit coupling. The Γ_8 state arising from the Γ_5 orbital state is also coupled to the Γ_8^* state arising from the Γ_4 orbital state by the same spin–orbit coupling interaction. The energy matrices for the Γ_7, Γ_8, and Γ_6 states are

$$\Gamma_7:\begin{vmatrix} 0 & \sqrt{3k}\zeta \\ \sqrt{3k}\zeta & \Delta-\frac{1}{2}k\zeta \end{vmatrix}$$

$$\Gamma_8:\begin{vmatrix} \Delta+\frac{1}{4}k\zeta & \frac{3}{4}\sqrt{5kk'}\zeta \\ \frac{3}{4}\sqrt{5kk'}\zeta & \Delta+\Theta-\frac{3}{4}k'\zeta \end{vmatrix}$$

$$\Gamma_6:\left|\Delta+\Theta+\frac{3}{2}k'\zeta\right| \quad (1)$$

Here ζ is the spin–orbit coupling constant, and k and k' are the orbital reduction factors for an electron in a Γ_5 orbital state and Γ_4 orbital state, respectively. Diagonalization of the energy matrix

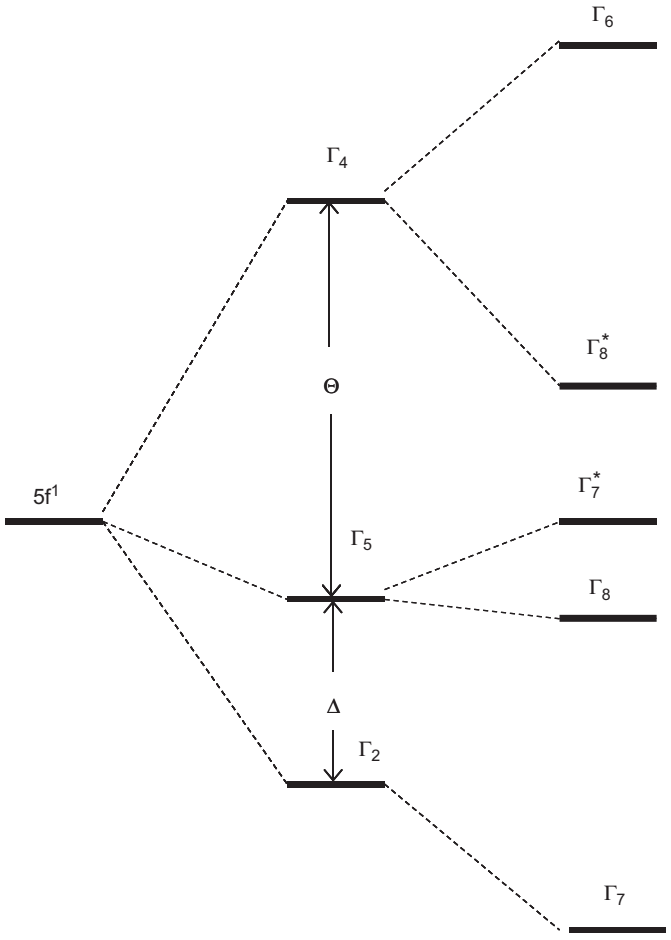

Fig. 4. Splitting of f^1 orbital energy levels perturbed by octahedral crystal field and spin–orbit coupling.

produces the ground state Γ_7 and the excited Γ_7', and the corresponding wavefunctions are written as

$$|\Gamma_7\rangle=\cos\theta|^2F_{5/2},\Gamma_7\rangle-\sin\theta|^2F_{7/2},\Gamma_7^*\rangle$$
$$|\Gamma_7'\rangle=\sin\theta|^2F_{5/2},\Gamma_7\rangle+\cos\theta|^2F_{7/2},\Gamma_7^*\rangle \quad (2)$$

where θ is the parameter describing the admixture of the Γ_7 levels in the ground state with the relation

$$\tan2\theta=\frac{2\sqrt{3k}\zeta}{\Delta-(1/2k\zeta)} \quad (3)$$

The g value for the ground Γ_7 doublet is obtained as follows:

$$g=2\langle\Gamma_7|\mathbf{L}+2\mathbf{S}|\Gamma_7\rangle=2\cos^2\theta-4\sqrt{\frac{k}{3}}\sin2\theta-\frac{2}{3}(1-k)\sin^2\theta \quad (4)$$

This g value is experimentally determined by the electron paramagnetic resonance (EPR) spectrum measurements. In this study, we tried to measure the EPR spectrum for $Ba_2U_2O_7$. However, no EPR spectrum was measured even at 4.2 K. Lewis et al. [12] also reported that no EPR signal from the U^{5+} ion could be detected in concentrated alkali metal uranates. This is probably because of the strong magnetic interaction between uranium ions (rapid spin–spin interaction) in the concentrated compounds. As will be described later, the g value for the ground doublet Γ_7 is also determined for the temperature-dependent part of the susceptibility. The energies for the Γ_7, Γ_8, Γ_7', Γ_8', and

Γ_6 (in the order of ascending energies) are

$$E(\Gamma_7) = \Delta - \frac{1}{2}\left\{k + 2\sqrt{3k}\cot\theta\right\}\zeta$$
$$E(\Gamma_8) = \Delta + \Theta - \frac{3}{4}\left\{k' + \sqrt{5kk'}\cot\varphi\right\}\zeta$$
$$E(\Gamma_7') = \sqrt{3k}\zeta\cot\theta$$
$$E(\Gamma_8') = \Delta + \frac{1}{4}\left\{k + 3\sqrt{5kk'}\cot\varphi\right\}\zeta$$
$$E(\Gamma_6) = \Delta + \Theta + \frac{3}{2}k'\zeta \quad (5)$$

where φ is the parameter describing the admixture of the Γ_8 levels in the excited state. We apply the above-mentioned treatments to the energy level analysis for $Ba_2U_2O_7$.

Since the effective magnetic moment of the U^{5+} ion is found to be 0.73 μ_B from the temperature-dependent part of the susceptibility, the g value is calculated to be 0.84 assuming the relation $\mu_{eff} = g\sqrt{S(S+1)}$. This g value is reasonable for an f^1 electron in an octahedral crystal field [13–16] and is often found for U^{5+} compounds [12,14,15,17–19]. It is worth noting that the sign of the g value is expected to be negative for this $5f^1$ electronic configuration [13–16]. As is described later, the calculation result using Eq. (4) gives a negative g value for this $Ba_2U_2O_7$ compound.

Now, we can use both the optical absorption spectrum and magnetic susceptibility data (the effective magnetic moment) to analyze the crystal field energy levels. The crystal field parameters and orbital reduction factors obtained are listed in Table 1. The spin–orbit coupling constant is 1954 cm^{-1}, which is a reasonable value for U^{5+} ion in solids, and is close to the value obtained from linear interpolation of the ζ values between Pa^{4+} and Np^{6+} compounds, 1950 cm^{-1} [20]. The obtained orbital reduction factor, $k' = 0.80$, for an electron in a Γ_4 orbital has also been calculated for the same Γ_4 orbital in $Ba_3MU_2O_9$ (M=Ca, Sr, Zn) and MUO_3 (M=L, Na, K, Rb) compounds [21–24]. As shown in Table 1, the transition energies calculated from these crystal field parameters and the g value of EPR (effective magnetic moment) are fitted to the experimental data except the $\Gamma_7 \rightarrow \Gamma_8'$ transition. Since the transition the $\Gamma_7 \rightarrow \Gamma_8'$ transition for octahedral symmetry is known to be broad and since this transition is furthermore broadened even due to small crystal field distortion, we have considered the $\Gamma_7 \rightarrow \Gamma_8'$ transition energy to be the least reliable.

Since we have obtained the wavefunctions and energies for the ground and excited states, the magnetic susceptibility of $Ba_2U_2O_7$ is easily calculated. The magnetic susceptibility of the molecule is given by

$$\chi = \frac{N\sum_{n,m}\{(E_{n,m}^{(1)})^2/k_BT - 2E_{n,m}^{(2)}\}\exp(-E_{n,m}^{(0)}/k_BT)}{\sum_{n,m}\exp(-E_{n,m}^{(0)}/k_BT)} \quad (6)$$

where N is the Avogadro number, $E_{n,m}^{(0)}$ is the zero-field energy, $E_{n,m}^{(1)}$ and $E_{n,m}^{(2)}$ are the first- and second-order Zeeman terms respectively, n and m are quantum numbers and k_B is the Boltzmann constant. If the separation of levels within the ground state is much smaller and the energy of the next excited state is much larger than kT, the susceptibility is expressed in the following form [25]:

$$\chi = \frac{Ng^2\mu_B{}^2}{4k_BT} + \chi_{TIP} \quad (7)$$

where

$$\chi_{TIP} = 2N\beta^2\sum_i \frac{|\langle\Gamma_i|\mathbf{L}+2\mathbf{S}|\Gamma_7\rangle|^2}{E(\Gamma_i)-E(\Gamma_7)} \quad (8)$$

The g value in Eq. (7) is the same as that for the ground crystal field state Γ_7 (Eq. (4)), i.e., the g value can be determined from the temperature-dependent part of the susceptibility, as described already.

Next, we will consider the temperature-independent susceptibility. From Eq. (8), it is calculated to be 204×10^{-6} emu/mol, which is near the experimentally estimated value, 140×10^{-6} emu/mol. As shown in Fig. 3, the calculated magnetic susceptibilities are in accordance with the experimental results in the paramagnetic temperature region.

3.2.2. Magnetic behavior below 58 K

The temperature dependence of the magnetic susceptibility for $Ba_2U_2O_7$ (Fig. 2) shows that there exist three magnetic anomalies. When the temperature is decreased through 58 K, the increment of the susceptibility differs among applied magnetic field. In addition, steep increase and small increase of the susceptibility has been observed at 19 and 8 K, respectively.

Fig. 5 shows the results of the specific heat measurements (temperature dependence of the specific heat divided by temperature (C_p/T)) for $Ba_2U_2O_7$. A λ-type specific heat anomaly has been observed at 19 K, corresponding to the results of magnetic susceptibility. These results clearly indicate that with decreasing temperature, $Ba_2U_2O_7$ undergoes a long-range antiferromagnetic transition at 19 K. In order to estimate the magnetic entropy change (ΔS_m) due to this transition, the magnetic entropy (S_m) was calculated by $S_m = \int C_m/T\,dT$. The magnetic specific heat (C_m) was obtained by subtracting the contribution of lattice specific

Table 1
Crystal field parameters and orbital reduction factors for $Ba_2U_2O_7$.

	Experimental	Calculation
$\Gamma_7 \rightarrow \Gamma_8$ (cm^{-1})	5634	5635
$\Gamma_7 \rightarrow \Gamma_7'$ (cm^{-1})	7194	7195
$\Gamma_7 \rightarrow \Gamma_8'$ (cm^{-1})	9852 (8696–13,158)	12,122
$\Gamma_7 \rightarrow \Gamma_6$ (cm^{-1})	15,873	15,873
g value	$\lvert g\rvert = 0.835$	−0.835
ζ (cm^{-1})		1954
Δ (cm^{-1})		3409
Θ (cm^{-1})		7151
k		1
k'		0.8

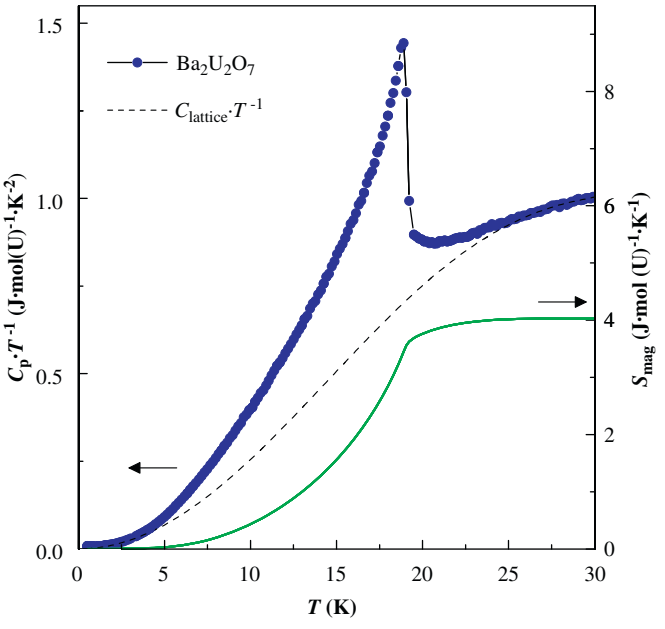

Fig. 5. Temperature dependence of the specific heat divided by temperature (C_p/T) and magnetic entropy (S_{mag}) for $Ba_2U_2O_7$ in the temperature region between 1.8 and 30 K.

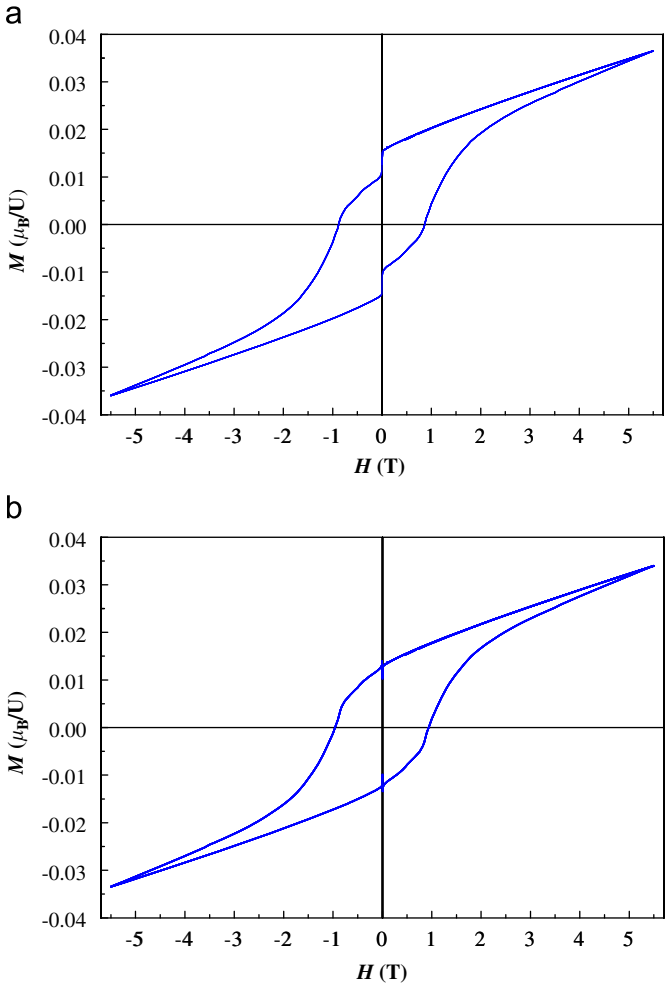

Fig. 6. (a) Magnetization (M) vs. H plot of $Ba_2U_2O_7$ measured at 2 K. (b) The modified magnetization curve in which a soft ferromagnetic component ($\sim 2.5\times10^{-3}\ \mu_B$/U) is extracted from the measured magnetization curve (see text).

heat from the observed specific heat. The lattice contribution was estimated by fitting a polynomial function of the temperature $f(T)=aT^3+bT^5+cT^7$ [26] to the observed specific heat data (T=26–30 K). The obtained magnetic entropy is also plotted in Fig. 5. The magnetic entropy change ΔS_m due to the antiferromagnetic transition is determined to be $\sim$4 J/mol(U) K, which is somewhat small but comparable to $R\ln 2=5.76$ J/mol(U) K (R: gas constant) expected from the doublet ground state of U^{5+} ion.

Fig. 6(a) shows the magnetization curve of $Ba_2U_2O_7$ against applied magnetic field measured at 2 K. This curve contains two ferromagnetic components: a hysteresis loop with $1.25\times10^{-2}\ \mu_B$/U and soft ferromagnetic curve with $2.5\times10^{-3}\ \mu_B$/U. The modified magnetization curve, in which the soft ferromagnetic component is extracted from the magnetization data, is plotted in Fig. 6(b). The observed hysteresis loop corresponds to the divergence between ZFC and FC susceptibilities below 19 K. However, the value of the magnetization at H=5.5 T is 0.034 μ_B/U, and the magnetization does not saturate at 2.0 K. These results indicate that this small ferromagnetic component is attributed to a weak ferromagnetic moment associated with a canted antiferromagnetic ordering. On the other hand, the soft ferromagnetic component is corresponding to the small increase of the magnetic susceptibility at 8 K. However, the results of the specific heat measurements show no anomaly at this temperature. Therefore, we consider that the anomaly observed at 8 K may be due to the small amount (0.2–0.3%) of ferromagnetic impurity.

The origin of the magnetic field-dependence of the susceptibility measured at 58 K is, at present, not clear. The results of the specific heat measurements indicate that about 70% of the theoretical magnetic entropy $R\ln 2$ has been consumed by the antiferromagnetic ordering at 19 K. The magnetic anomaly which sets in at 58 K suggests the short range magnetic correlations. One possibility is that the anomaly at 58 K may be due to the onset of one-dimensional magnetic correlations associated with the linear chains formed by the U1 ions. Furthermore investigations are needed to elucidate the magnetic behavior observed at 58 K.

4. Summary

Magnetic susceptibility, magnetization and specific heat measurements reveal that $Ba_2U_2O_7$ undergoes a canted antiferromagnetic ordering at 19 K. The magnetic anomaly which sets in at 58 K may be due to one-dimensional magnetic correlations of the U ions. The magnetic susceptibility results and the optical absorption spectrum were analyzed on the basis of an octahedral crystal field model.

References

[1] Gmelin's Handbuch der Anorganischen Chemie, System-Nr55, U, Teil C3, Springer-Verlag, New York/Berlin, 1975.
[2] H. Kleykamp, J. Nucl. Mater. 131 (1985) 221–246.
[3] R.D. Shannon, Acta Crystallogr. Sect. A32 (1976) 751–767.
[4] E.H.P. Cordfunke, D.J.W. IJdo, J. Phys. Chem. Solids 49 (1988) 551–554.
[5] A. Nakamura, Y. Kenji, Physica B378–380 (2006) 548–549.
[6] R. Braun, S. Kemmler-Sack, H. Roller, I. Seeman, I. Wall, Z. Anorg. Allg. Chem. 415 (1975) 133–155.
[7] F. Izumi, T. Ikeda, Mater. Sci. Forum 198 (2000) 321–324.
[8] K. Momma, F. Izumi, J. Appl. Crystallogr. 41 (2008) 653–658.
[9] S.R. Dharwadkar, M.S. Chandrasekharaiah, Anal. Chim. Acta 45 (1969) 545–546.
[10] T. Fujino, T. Yamashita, Fresenius' Z. Anal. Chem. 314 (1983) 156.
[11] C. Keller, MTP international review of science, in: K.W. Bagnall (Ed.), Lanthanides and Actinides, Series I, vol. 7, Butterworths, London, , 1972.
[12] W.B. Lewis, H.G. Hecht, M.P. Eastman, Inorg. Chem. 12 (1973) 1634–1639.
[13] J.C. Eisenstein, M.H.L. Pryce, Proc. R. Soc. London A255 (1960) 181–198.
[14] C.A. Hutchison Jr., B. Weinstock, J. Chem. Phys. 32 (1960) 56.
[15] P. Rigny, A.J. Dianoux, P. Plurien, J. Phys. Chem. Solids 32 (1971) 1175–1180.
[16] Y. Hinatsu, T. Fujino, N. Edelstein, J. Solid State Chem. 99 (1992) 182–188.
[17] P. Rigny, P. Plurien, J. Phys. Chem. Solids 28 (1967) 2589–2595.
[18] M. Dryfford, P. Rigny, P. Plurien, Phys. Lett. A27 (1968) 620–621.
[19] J. Selbin, H.J. Sherrill, Inorg. Chem. 13 (1974) 1235–1239.
[20] J. Selbinm, J.D. Ortego, G. Gritzner, Inorg. Chem. 7 (1968) 976–982.
[21] Y. Hinatsu, J. Solid State Chem. 108 (1994) 356–361.
[22] Y. Hinatsu, J. Solid State Chem. 110 (1994) 118–123.
[23] Y. Hinatsu, J. Alloys Compd. 203 (1994) 251–257.
[24] Y. Hinatsu, J. Alloys Compd. 218 (1995) 58–63.
[25] J.H. van Vleck, Theory of Electric and Magnetic Susceptibilities, Clarendon, Oxford, 1932.
[26] J.E. Gordon, R.A. Fisher, Y.X. Jia, N.E. Phillips, S.F. Reklis, D.A. Wright, A. Zettl, Phys. Rev. B 59 (1999) 127–130.